Supplement of

The atmospheric settling of commercially sold microplastics

Alina Sylvia Waltraud Reininger et al.

Correspondence to: Alina Sylvia Waltraud Reininger (alina.reininger@univie.ac.at)

Chain of equations to calculate the drag coefficient C_d of freely falling non-spherical particles in liquids or gases based on the shape correction scheme of Bagheri and Bonadonna (2016; 2019):

$$C_D = \frac{24\,k_S}{Re}(1 + 0.125(Re\,k_N/k_S)^{2/3}) + \frac{0.46\,k_N}{1 + 5330/(Re\,k_N/k_S)} \tag{S1}$$

$k_{\mathrm{S,rand}}$, $k_{\mathrm{N,rand}}$, $k_{\mathrm{S,max}}$, and $k_{\mathrm{N,max}}$ are the Stokes' and Newton's drag corrections for random-orientation-drag and maximum-orientation-drag, respectively. Stokes' and Newton's drag corrections for average-orientation-drag, $k_{\mathrm{S,aver}}$, $k_{\mathrm{N,aver}}$, have been introduced by Tatsii et al. (2024).

$$k_{\mathrm{S,rand}} = (F_S^{1/3} + F_S^{-1/3})/2 \tag{S2}$$

$$k_{\mathrm{N,rand}} = 10^{\alpha_2(-\log(F_N))\beta_2} \tag{S3}$$

$$k_{\mathrm{S,max}} = (F_S^{0.05} + F_S^{-0.36})/2 \tag{S4}$$

$$k_{\mathrm{N,max}} = 10^{0.77(-\log(F_N))^{0.63}} \tag{S5}$$

$$k_{\mathrm{S,aver}} = (k_{\mathrm{S,max}} + k_{\mathrm{S,rand}})/2 \tag{S6}$$

$$k_{\mathrm{N,aver}} = (k_{\mathrm{N,max}} + k_{\mathrm{N,rand}})/2 \tag{S7}$$

α_2 and β_2 are empirical parameters that depend on the particle-to-fluid density ratio ρ':

$$\alpha_2 = 0.45 + \frac{10}{\exp(2.5\log\rho') + 30} \tag{S8}$$

$$\beta_2 = 1 - \frac{37}{\exp(3\log\rho') + 100} \tag{S9}$$

The simplified version of the model, which is suited for elongated particles, in contrast to the full version, neglects the term $\frac{d_{eq}^3}{L\,I\,S}$ in the Stokes' form factor F_S and in Newton's form factor F_N:

$$F_S = fl\,el^{1.3}\,(\frac{d_{eq}^3}{L\,I\,S}) \tag{S10}$$

$$F_N = fl^2\,el\,(\frac{d_{eq}^3}{L\,I\,S}) \tag{S11}$$

Microscopic images of the glitter particles and fibers recorded with a 3D laser microscope (VK-X200K, KEYENCE International (Belgium) NV/SA) are shown in Fig. S2 and Fig. S3. The dimensions of the glitter particles differ from those given by the manufacturer; therefore, from the microscopic images, L and I were extracted with the software ImageJ. L is defined as the longest dimension of the particle and I as the longest dimension of the particle perpendicular to L, according to the standard protocol proposed by Krumbein (1941). The shortest dimension, S, was evaluated with the 3D laser microscope, where the glitter particle's thickness was chosen as S, with S being perpendicular to both L and I. The dimensions of the fibers measured with the microscope agreed well with the properties given by the manufacturer. The arrows in Figure S1 depict examples of how L and I were chosen for glitter particles with irregular (a) and regular shapes (b) and for fibers (c).
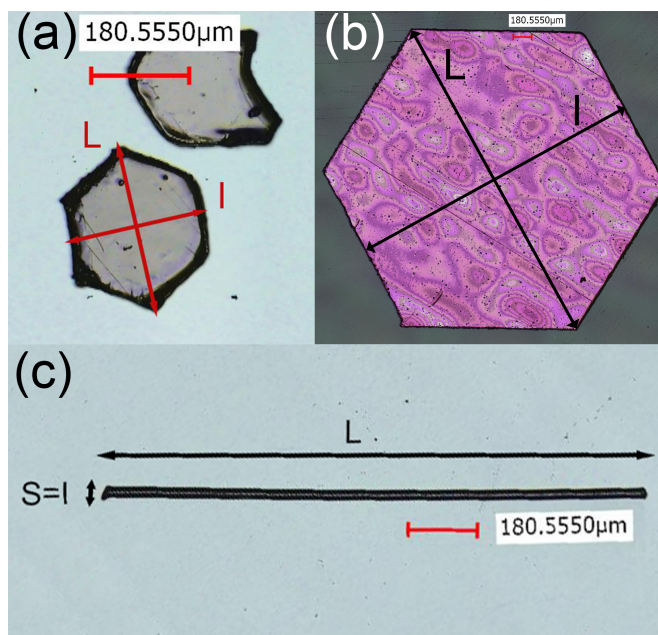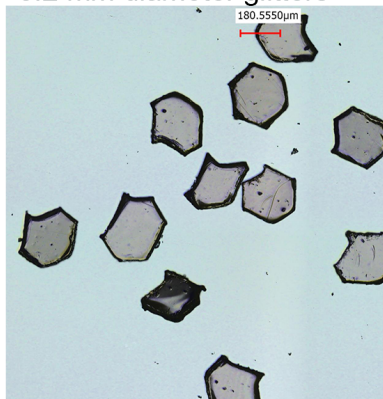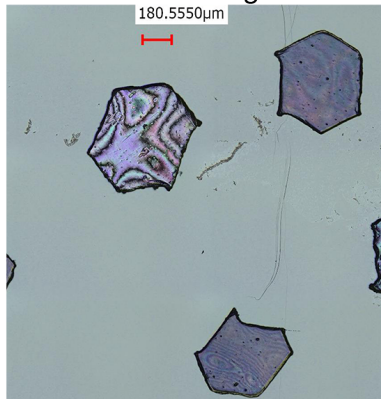

Figure S1. Longest L, intermediate I and shortest S dimension of the glitters (a), (b), and fibers (c). For films, the S dimension is represented by the film thickness.
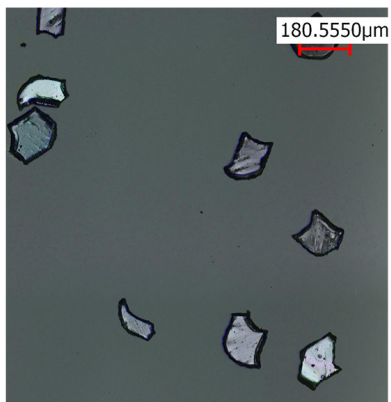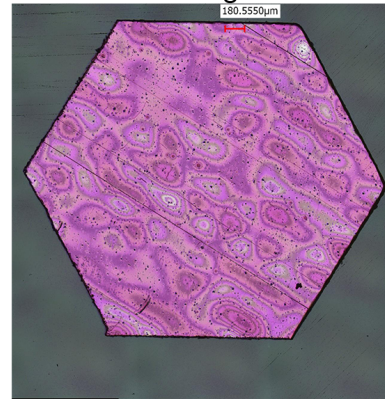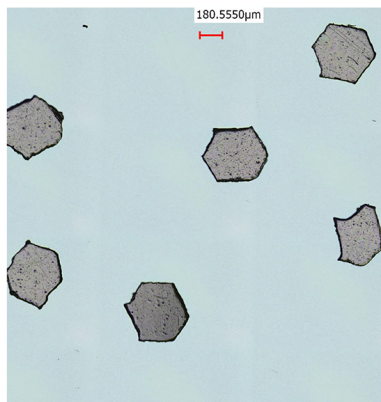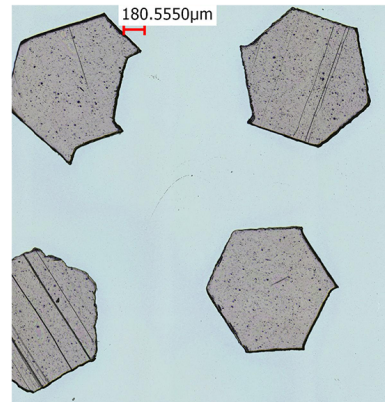
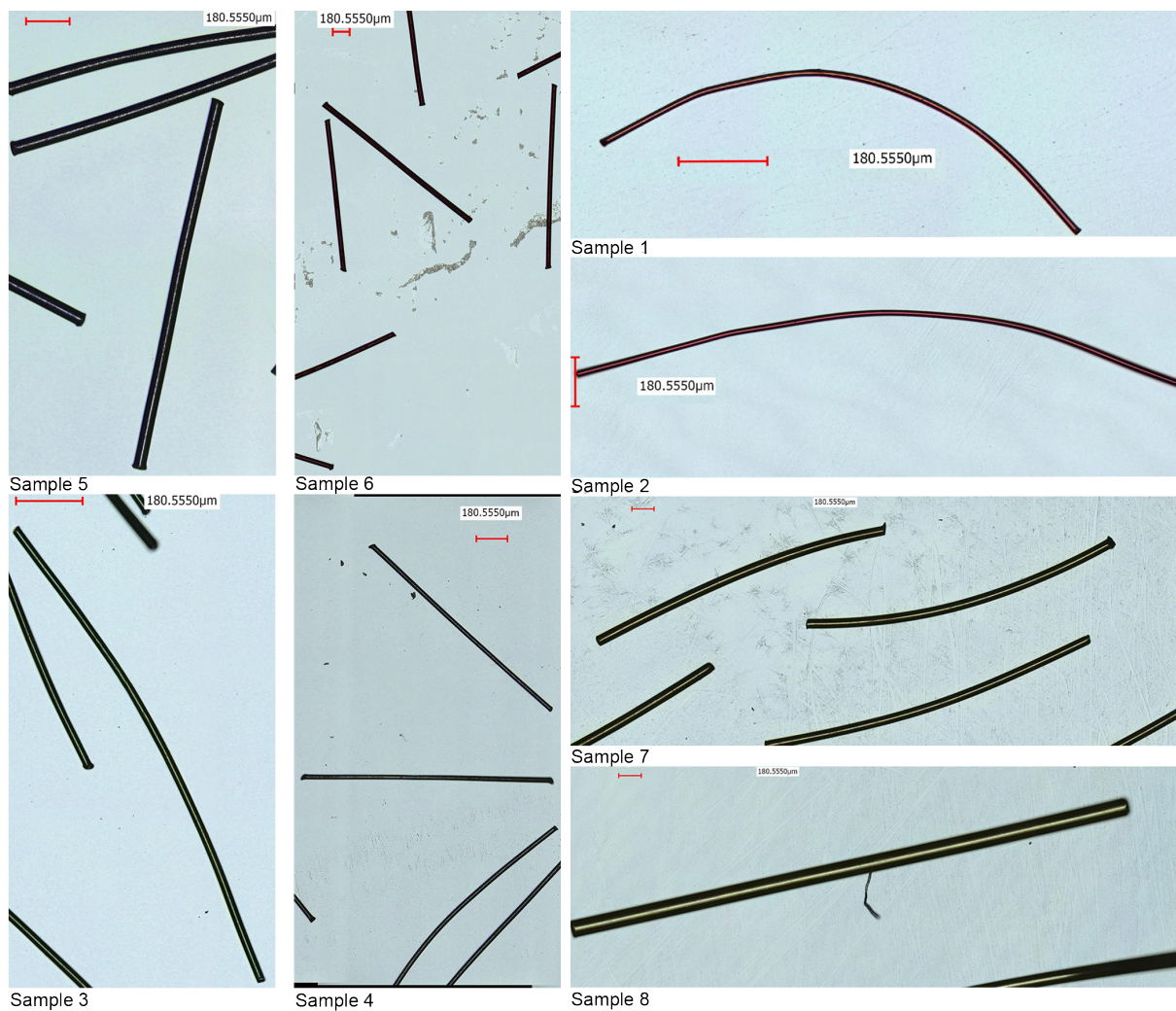**Figure S2.** Microscopic images of the glitter particles used in the experiments.

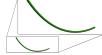**Figure S3.** Microscopic images of the fibers used in the experiments.

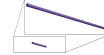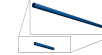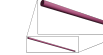**Table S1.** Simulation times for different FLEXPART runs.

Particle	Simulation time
0.05 mm diameter glitters	3 days
0.1 mm diameter glitters	10 h
0.2 mm diameter glitters	10 h
0.4 mm diameter glitters	5 h
0.6 mm diameter glitters	3 h
1 mm diameter glitters	2 h
3 mm diameter glitters	2 h
0.05 mm diameter spheres	3 days
0.1 mm diameter spheres	10 h
0.2 mm diameter spheres	3 h
0.4 mm diameter spheres	2 h
0.6 mm diameter spheres	2 h
1 mm diameter spheres	2 h
3 mm diameter spheres	2 h

Table S2. Wet scavenging parameters that have been varied for the sensitivity test: cloud condensation nuclei efficiencies (CCN), ice-nucleating particle efficiencies (IN), and scavenging efficiencies for rain (Crain) and snow (Csnow). The parameters were selected based on the values proposed by Evangeliou et al. (2020) and Wang et al. (2014). Indicated are additionally the relative differences averaged over all particle sizes between the base simulations and sensitivity analyses.

	CCN	IN	Crain	Csnow	Mean rel. difference travel distances (%)	Mean rel. difference residence times (%)
Base simulation	0.001	0.01	1	1	-	-
High CCN	0.5	0.01	1	1	1.93	3.38
High IN	0.001	0.8	1	1	1.86	4.01
Low Crain	0.001	0.01	0.6	1	1.71	3.82
Low Csnow	0.001	0.01	1	0.5	1.87	3.79

Table S3. Settling velocities of fibers; experimental (v_t), and modeled (v_{max}, v_{aver}, v_{rand}) with the simple version of Bagheri and Bonadonna's (2016; 2019) model [a]

Name	Sample 1	Sample 2	Sample 3	Sample 4	Sample 5	Sample 6	Sample 7	Sample 8
Symbol								
v_t (m/s)	0.03	0.07	0.07	0.11	0.25	0.25	0.38	0.62
σ_{vt} (m/s)	0.01	0.01	0.01	0.01	0.02	0.20	0.02	0.09
v_{max} (m/s)	0.02	0.07	0.09	0.10	0.24	0.25	0.40	0.64
v_{aver} (m/s)	0.02	0.08	0.10	0.12	0.27	0.28	0.45	0.72
v_{rand} (m/s)	0.03	0.09	0.11	0.13	0.31	0.32	0.53	0.86

[a] The measured velocity v_t is given as the average over the number of experiments of the corresponding shape and size, with σ_{vt} being the standard deviation. v_{rand}, v_{max}, v_{aver} are the modeled velocities with random-, maximum-, and average-orientation-drag configuration, respectively.
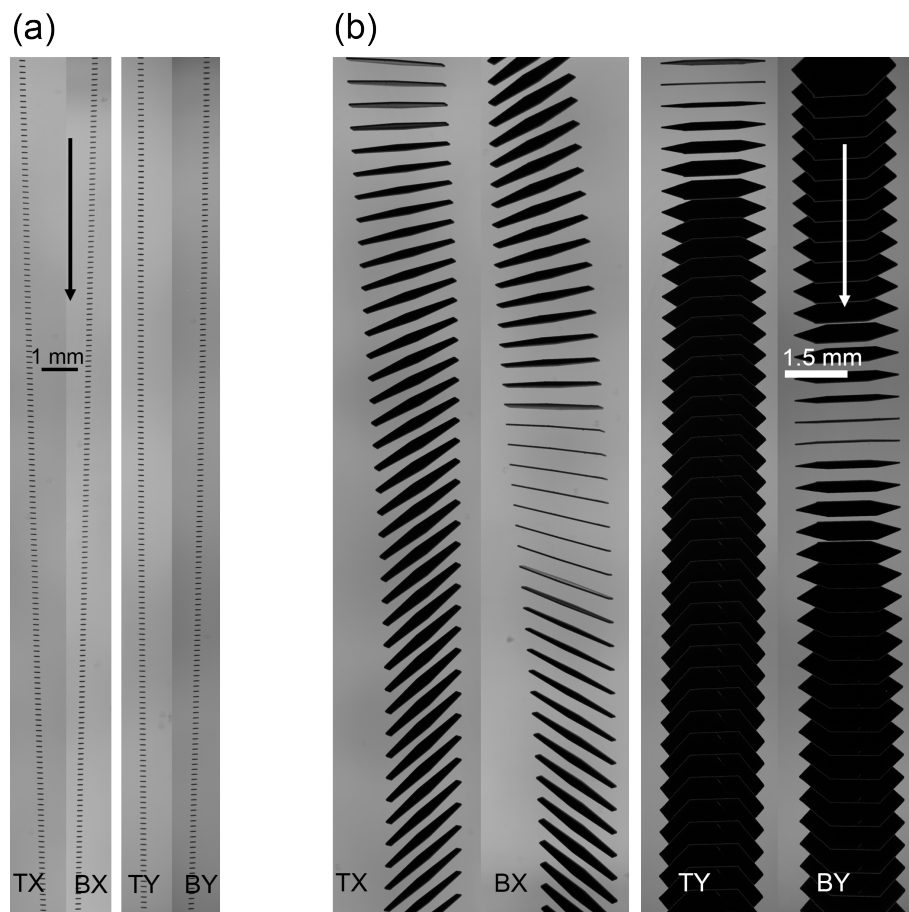
Figure S4. Experimental recording of the gravitational settling behavior of glitters with nominal diameters of 0.1 mm (a) and 3 mm (b). For each glitter particle, data from the two upper cameras (TX and TY) and the two lower cameras (BX and BY) for the entire vertical length of the cameras' observation volumes is shown.

Figure S5. Experimental recording of the gravitational settling behavior of fibers of sample 6 (a) and sample 4 (b). For each fiber, data from the two upper cameras (TX and TY) and the two lower cameras (BX and BY) for the entire vertical length of the cameras' observation volumes is shown.
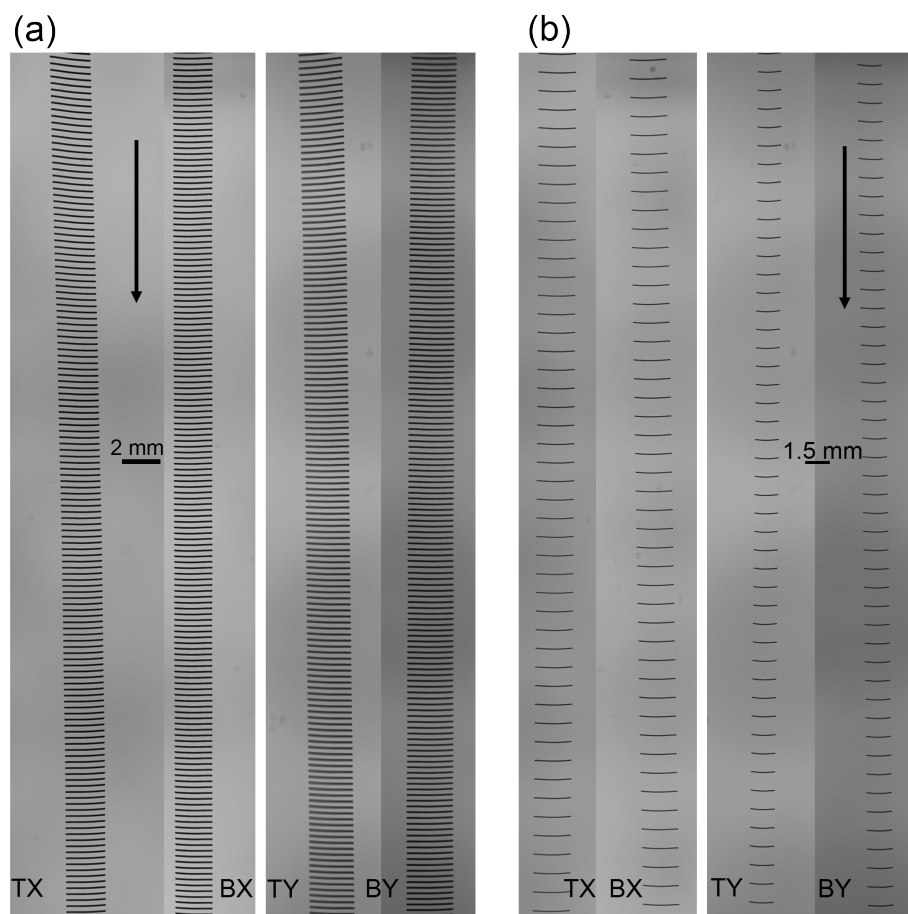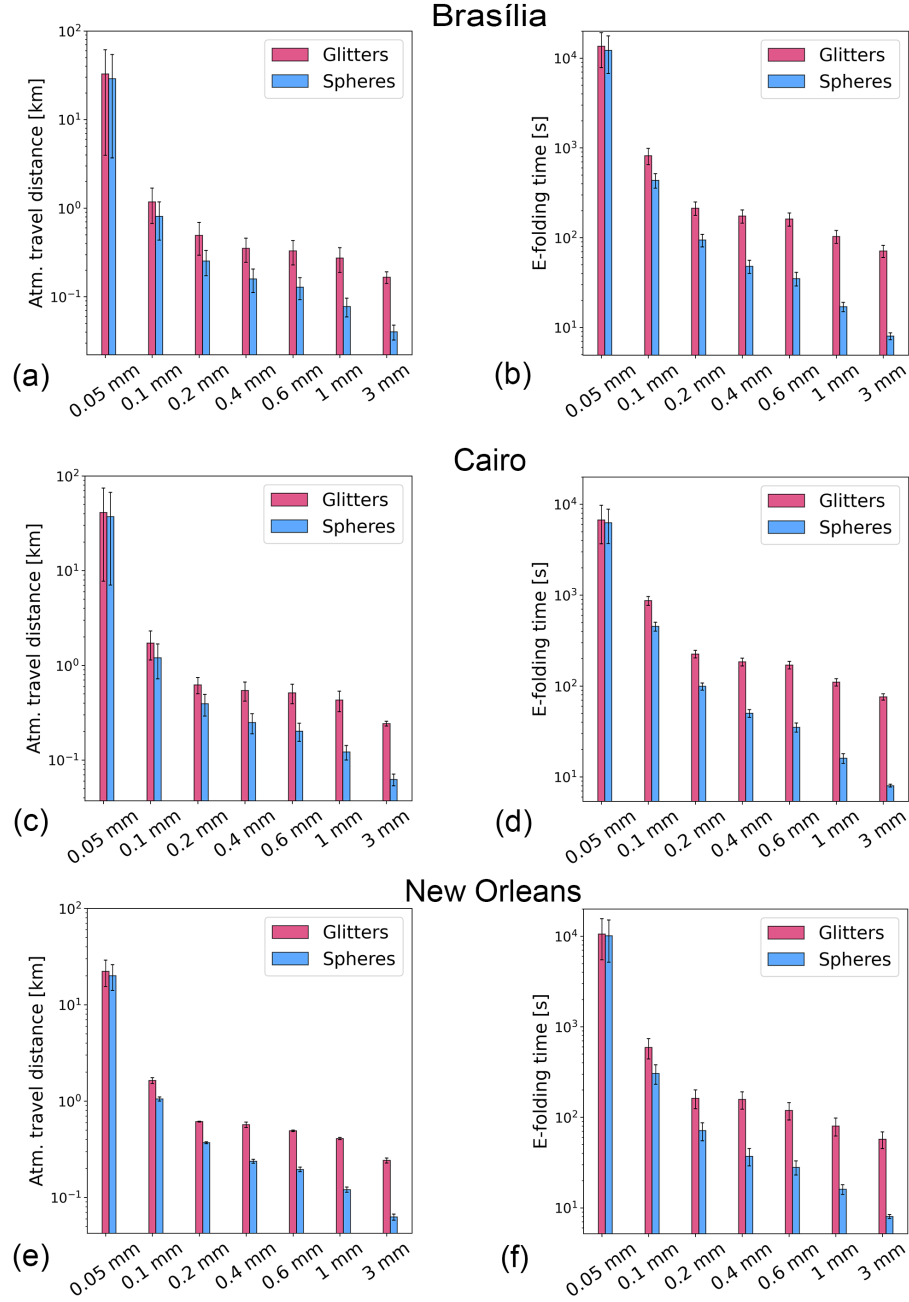
Figure S6. Mean atmospheric horizontal travel distances and atmospheric residence times of glitters (pink) and volume equivalent spheres (blue) for the release points Brasília (a), (b), Cairo (c), (d), and New Orleans (e),(f). Standard deviations are depicted by whiskers.
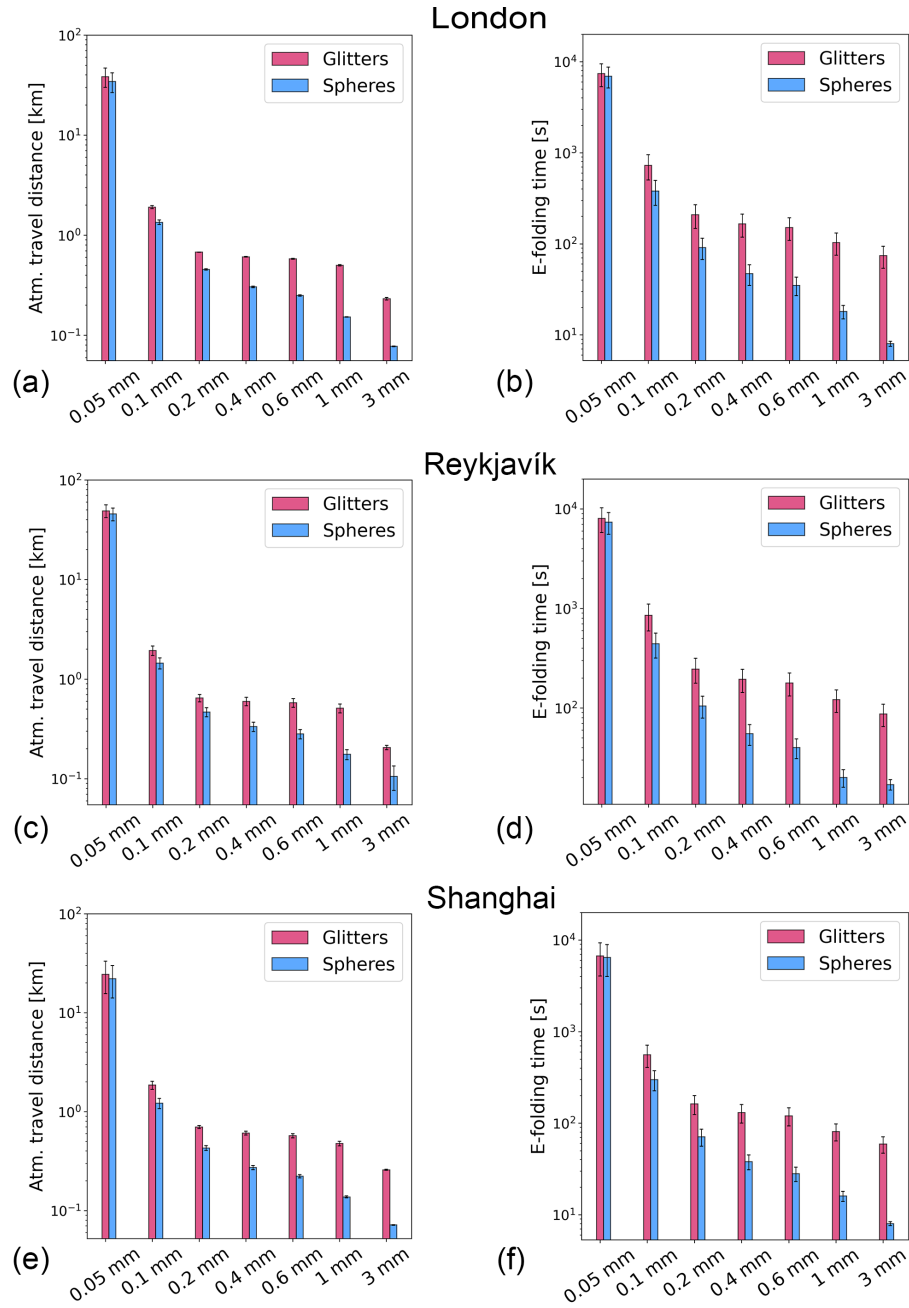
Figure S7. Mean atmospheric horizontal travel distances and atmospheric residence times of glitters (pink) and volume equivalent spheres (blue) for the release points London (a), (b), Reykjavík (c), (d), and Shanghai (e),(f). Standard deviations are depicted by whiskers.

References

Bagheri, G. and Bonadonna, C.: On the drag of freely falling non-spherical particles, Powder Technol., 301, 526–544, https://doi.org/10.1016/j.powtec.2016.06.015, 2016.

Bagheri, G. and Bonadonna, C.: Erratum to "On the drag of freely falling non-spherical particles" [Powder Technology 301 (2016) 526–544, DOI: 10.1016/j.powtec.2016.06.015], Powder Technol., 349, 108, https://doi.org/10.1016/j.powtec.2018.12.040, 2019.

Evangeliou, N., Grythe, H., Klimont, Z., Heyes, C., Eckhardt, S., Lopez-Aparicio, S., and Stohl, A.: Atmospheric transport is a major pathway of microplastics to remote regions, Nat. Commun., 11, https://doi.org/10.1038/s41467-020-17201-9, 2020.

Krumbein, W.: MEASUREMENT AND GEOLOGICAL SIGNIFICANCE OF SHAPE AND ROUNDNESS OF SEDIMENTARY PARTI-CLES, J. Sediment. Res., 11, 64 – 72, https://doi.org/10.1306/D42690F3-2B26-11D7-8648000102C1865D, 1941.

Tatsii, D., Bucci, S., Bhowmick, T., Guettler, J., Bakels, L., Bagheri, G., and Stohl, A.: Shape Matters: Long-Range Transport of Microplastic Fibers in the Atmosphere, Environ. Sci. Technol., 58, 671–682, https://doi.org/10.1021/acs.est.3c08209, 2024.

Wang, X., Zhang, L., and Moran, M. D.: Development of a new semi-empirical parameterization for below-cloud scavenging of size-resolved aerosol particles by both rain and snow, Geosci. Model Dev., 7, 799–819, https://doi.org/10.5194/gmd-7-799-2014, 2014.